

Chapter 7

Buckling Delamination of Compressed Thin Films

Myoung-Woon Moon

Abstract The aim of this chapter is to review the studies on buckle delamination in compressively stressed thin films over substrates by pulling together experimental and theoretical analysis. The general phenomena shown in delamination buckles of compressively stressed films were discussed from the onset to propagation over the substrates. The experimental observations were characterized by the delamination conditions and buckle morphologies. Then, the related mechanics for buckle delamination were provided with a theoretical solution for simple buckle configurations and a numerical solution for nonlinear buckle. Based on the experimental and theoretical analysis, the buckle configuration was applied to fluidic channels by precisely controlling buckle width within the desired area by adjusting interface adhesion.

7.1 Introduction

When the strain energy of a compressive film exceeds the interface toughness or interface adhesion energy, the film could show the interesting nonlinear behavior of buckle delamination. Nonlinear configurations of delamination buckle have been observed in many different film–substrate systems under residual compressive stress of up to several GPa, which developed from the thermal expansion coefficient mismatch or lattice parameter mismatch between film and substrate, or intrinsic stress from its bonding structure which originated during deposition [4, 8, 20]. When the film or skin is well adhered to its substrate which is relatively compliant, like polymers (e.g., PMMA, PDMS), then buckle of the thin film or skin without delamination against the substrate has been reported even under high compression

M.-W. Moon (✉)

Future Convergence Research Division, Korea Institute of Science and Technology (KIST),
Seoul, Republic of Korea
e-mail: mwmoon@kist.re.kr

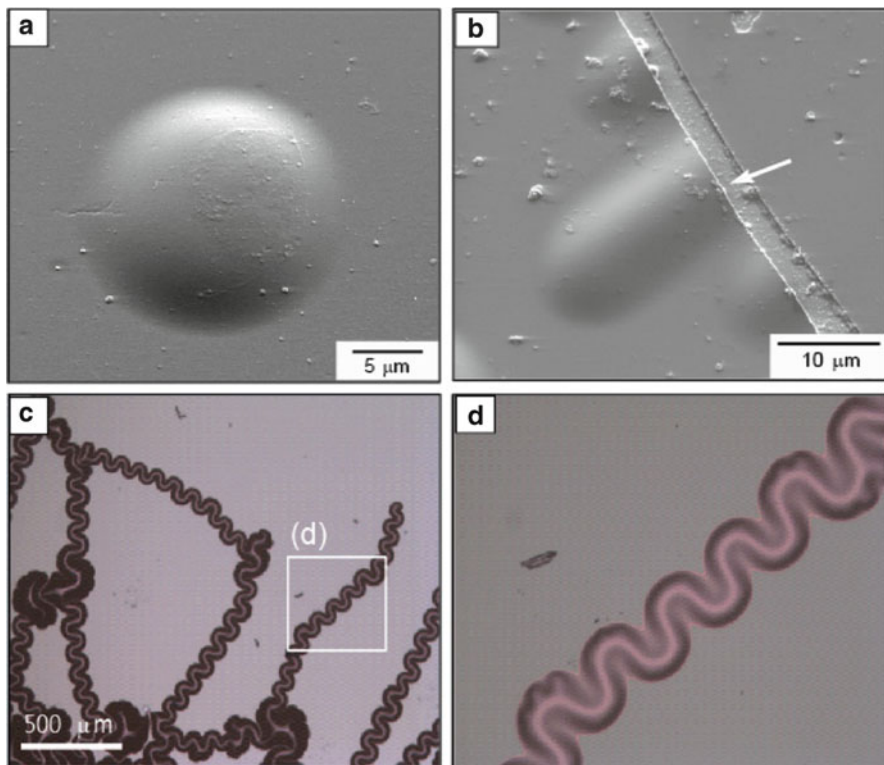


Fig. 7.1 Buckle configurations of three categories; a circular buckle (a), a straight-sided buckle (b), and a nonlinear telephone cord buckle (c, d)

[2, 3, 23]. However, on moderate substrates like glass, Si, or metal, compressively stressed films are likely to delaminate into the buckle configuration, which would further enhance the delamination [7, 19–21].

Several systems under compressive stress have been reported to reveal the buckle configuration as the stress relief pattern. With high residual stress, diamond-like carbon (DLC) films or diamond films on glass, Si, or steel have been well known for delamination buckle configurations [16, 18, 21, 29], as well as such systems as mica films glued on Al, Mo films on glass [12, 25], amorphous (hydrogenated) Si films on glass/Si [27], stainless steel on polycarbonate, Fe/Ni compositionally modulated films, Boron films on NaCl [14, 15], and Nickel films on polycarbonate substrates. Hydrogen-enhanced niobium (Nb) films on polycarbonate (PC) or mica have buckle geometries due to increased hydrogen concentration [26].

In the presence of small interface separations, the films may buckle to release the strain energy or residual stress. The ensuing buckles of engineering films on substrates exhibit several configurations, ranging from circular to linear to telephone cord as summarized in Fig. 7.1. The linear symmetric types, such as circular buckle (Fig. 7.1a) or straight-sided buckle (Fig. 7.1b) initiated along the free edge,

would be rarely observed in experimental conditions due to their energetic stability, while the nonlinear and asymmetric morphology of buckle (Fig. 7.1c, d), the so-called telephone cord buckle, has been well reported in many systems [20, 22]. Note that nonlinear buckle, or telephone cord buckle, has a nonlinear side configuration, which is periodically repeated with an asymmetric unit segment. However, buckles known as straight-sided buckle and circular buckle show symmetric and linear configurations, but are rare in real experimental conditions due to their energetic instability.

In this chapter, the experimental observations were reviewed for the delamination condition and buckle morphologies. Then, the related mechanics for buckle delamination were reviewed with a theoretical solution for simple buckle configurations and a numerical solution for nonlinear buckle. The role of imperfections on the initiation and propagation of buckle-driven delaminations in compressed thin films has been demonstrated by experiments performed with DLC films deposited onto glass substrates. The surface topologies and interface separations have been characterized using the Atomic Force Microscope (AFM) and the Focused Ion Beam (FIB) imaging systems.

The profiles of several nonlinear buckles have been measured to establish the symmetry of each repeated unit, revealing similarity with a circular buckle pinned at its center. Lithographic techniques applied to a substrate prior to film deposition can create areas of low interface adhesion surrounded by regions of high adhesion. When the area of low adhesion is a strip, the width of the strip controls the buckle morphology: smooth Euler buckles for narrow strips, telephone cord buckles for wider strips, and symmetric varicose buckles under a very limited range of conditions. A complex and designed pattern of buckling delamination has been introduced for simple fluidic applications.

It has been shown that the telephone cord topology can be effectively modeled as a series of pinned circular buckles along its length, with an unpinned circular buckle at its front. Furthermore, evaluation of the energy state over the buckle unit or the energy release rate at the crack tip along the nonlinear side is conducted with 3-D numerical models.

7.2 Buckling Delamination of Thin Compressed Films

7.2.1 Imperfection-Driven Delamination Buckling

Delamination or buckle would be caused near the interface defects or free edge (Fig. 7.1) [20] with critical imperfection length due to unstable stress or strain energy. The failure responses exhibited by residually compressed thin films on thick substrates have been widely documented [5, 19, 20, 28]. Most typically, in the presence of small interface separations, the films may buckle and, moreover, the buckles can propagate beneath the film if the induced energy release rate exceeds

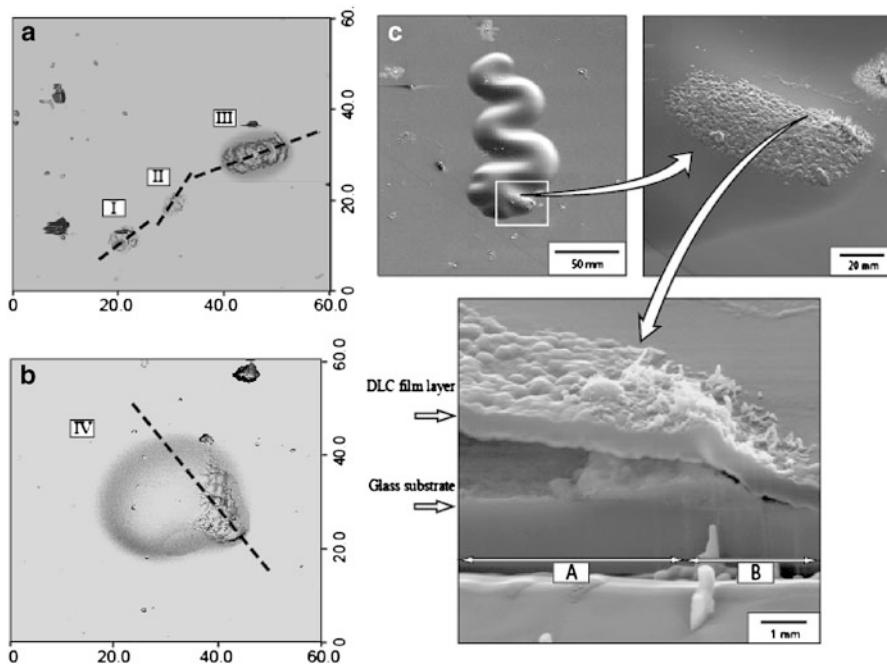


Fig. 7.2 AFM surface profiles of four imperfections. Images of three imperfections (a) (*I, II, III*) with small diameter and a large one (b) (*IV*). (c) SEM images with side and cross-sectional views for before and after sectioning with the FIB. Moon et al. [20], reprinted with permission

the interface fracture toughness. Since the initiation of the buckles would start from delamination of films at the interfaces that have defects, failures induced by imperfections or defects should be understood in detail.

As in all practical buckling problems, imperfections at the interfaces are expected to be important and some effects of geometric imperfections have been analyzed by either theory or experiment [11, 20]. In brief summary, the energy release rate, G , for an interface separation beneath the imperfection is dramatically altered, relative to a flat surface. Most importantly, a finite G develops even for very small initial separations and is attributed to the tensile stress normal to the interface. Measurements of the surface defects of coatings, reflected off interfacial defects, have been performed on the imperfections analyzed with AFM surface profiling and FIB cross sectioning as shown in Fig. 7.2 [20].

Briefly, the conditions for the deposition of DLC films on standard microscope slides made from soda lime glass were the following [20]. The DLC films were deposited using a capacitively coupled r.f. glow discharge, choosing conditions that generate delamination buckles. By applying a negative self-bias voltage controlled in the range of -100 to -700 V, the film thickness was in the range of 0.26 – 0.46 μm , and the residual compression was between about 1 and 4 GPa, resulting in delamination buckles with wavelengths of about 20 – 25 μm . Various

surface topologies appear (Fig. 7.2a, b), indicative of a range of imperfections. It will be shown that these imperfections are all related to defects on the surface of the glass prior to DLC deposition.

AFM measurements were performed on the imperfection sites as shown in Fig. 7.2a, b. The AFM surface profiles reveal four imperfection categories. The differing profiles suggest the three basic responses shown schematically in Fig. 7.2a–c. The two smaller imperfections (numbers I and II) both have amplitudes of around 140 nm and wavelengths of about 6.2 μm . Their irregular profiles indicate that the DLC is still fully attached to the substrate, having imperfections of similar shape to those at the interfaces between film and substrate. The relatively larger imperfection (number III in Fig. 7.2a) has a substantially different profile. The irregular segment on the right (with features similar to imperfections I and II) appears to separate and buckle from the interface. The largest imperfection (number IV on Fig. 7.2b) appears at the source of a propagating telephone cord buckle. The imperfection size is determined to have amplitude, $\delta = 360$ nm and wavelength, $L_0 = 20.0$ μm .

In all cases shown above, note that the irregular topology found on the surface reflects the initial topology of the substrate, affirming that the DLC deposits everywhere with uniform thickness, $h = 0.46$ μm . Images of a larger imperfection that initiated a telephone cord buckle (Fig. 7.2c) reveal the separation. The amplitude of this imperfection exceeds the film thickness, $\delta = 1.2h$. It is also asymmetric. Region “A” on the left has a larger wavelength, $L_1 \approx 60h$. This is also the side that dictates the direction in which the buckle propagates. In region “B” on the right, the imperfection wavelength is smaller, $L_2 = 18h$, and the buckle is stationary.

7.2.2 Buckling Delamination of Compressed Thin Films

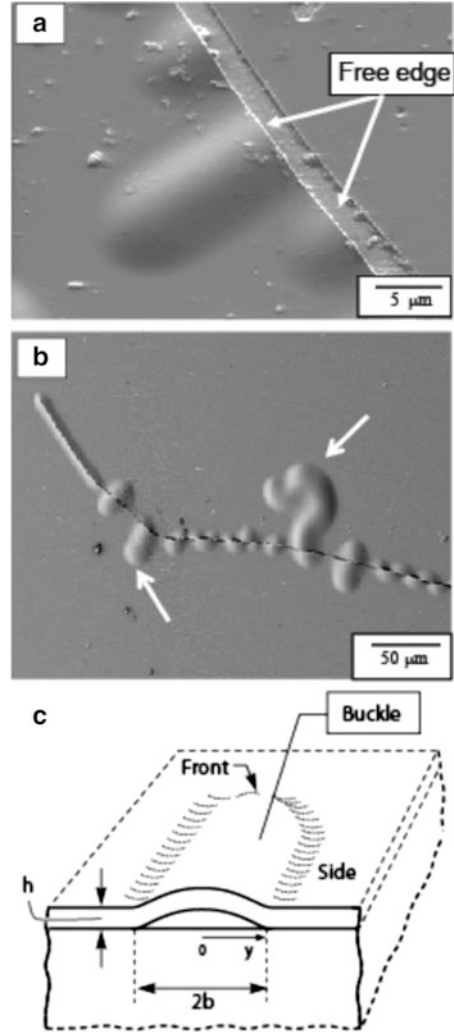
7.2.2.1 Linear Buckling Instability

The buckles propagate beneath the film if the induced energy release rate exceeds the interface fracture toughness. The associated mechanics have been well documented [9]. The buckles exhibit several configurations, from circular to linear to telephone cord (Figs. 7.1a and 7.3). *Straight buckles* propagate with a curved front. The conditions at the stationary side and the circular front have been modeled and rationalized in terms of mode mixity and energy release rate [9, 10, 13].

For thin films of thickness h , subject to equi-biaxial compression, σ_0 , the surface displacement w normal to the substrate of a *straight-sided buckle* (Fig. 7.3c), as a function of distance y measured from the middle of the buckle well behind the curved front, is given by [9]

$$\frac{w}{h} = \frac{\xi}{2} \left(1 + \cos\left(\frac{\pi y}{b}\right) \right), \quad (7.1)$$

Fig. 7.3 Straight-sided buckles initiated from free edge (a) and buckling transition from straight to telephone cord (arrow-marked) (b). A schematic for modeling a straight-sided buckle (c)



where $2b$ is the width and

$$\xi \equiv \frac{w_{\max}}{h} = \sqrt{\frac{4}{3} \left(\frac{\sigma_0}{\sigma_c} - 1 \right)}. \quad (7.2)$$

The critical bifurcation stress, σ_c , at width $2b$, is

$$\sigma_c = \left(\frac{\pi^2}{12} \right) \frac{E}{1 - \nu^2} \left(\frac{h}{b} \right)^2 \quad (7.3)$$

with E and ν the Young's modulus and Poisson's ratio of the film, respectively. The energy release rate and phase angle, $\tan\psi_s \equiv K_{II}/K_I$, on the sides, well behind the curved front, are

$$\frac{G_s}{G_0} = \left(1 - \frac{\sigma_c}{\sigma_0}\right) \left(1 + 3 \frac{\sigma_c}{\sigma_0}\right), \quad (7.4)$$

$$\tan\psi_s = \frac{4\cos\omega + \sqrt{3}\xi\sin\omega}{-4\sin\omega + \sqrt{3}\xi\cos\omega}, \quad (7.5)$$

where the energy release rate has been normalized by the strain energy per unit area when the film is released in plane strain [9]:

$$G_0 = \frac{(1 - \nu^2)h\sigma_0^2}{2E}. \quad (7.6)$$

Note that the normalized energy release rate, G/G_0 , and the maximum deflection, w_{\max}/h , depend only on the normalized stress, σ_0/σ_c . The phase angle, ψ , while also a function of the Dundurs' parameters [9], for present purposes is set to the value of absent elastic mismatch, whereupon $\omega = 52.1^\circ$.

The steady-state energy release rate averaged over the curved front is [9]

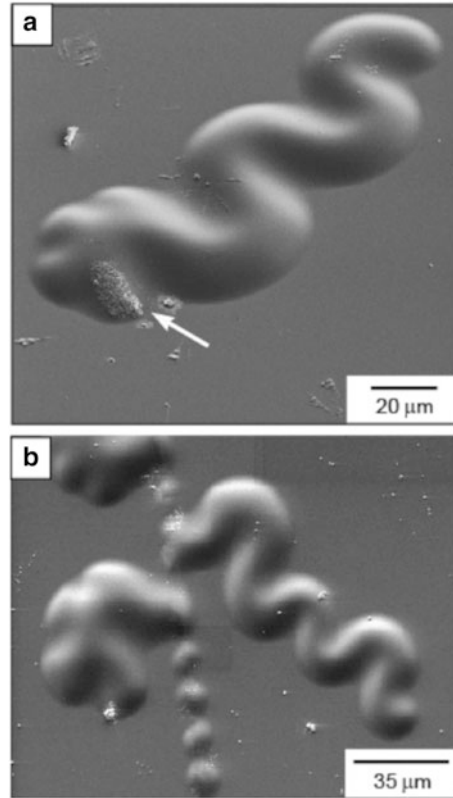
$$\frac{G_{ss}}{G_0} = \left(1 - \frac{\sigma_c}{\sigma_0}\right)^2. \quad (7.7)$$

The energy release rate along the sides exceeds that along the front at all σ_0/σ_c [10]. Yet, the front propagates because it experiences a significant opening mode, while the sides become exclusively mode II, once the buckle attains a characteristic width (associated with $\sigma_0/\sigma_c = 7.54$).

7.2.2.2 Nonlinear Buckling Instability

As the calculation for the nonlinear side of the stationary telephone cord buckle has been conducted, one can consider the propagation of buckles expanding through the entire film [21]. The formation mechanism of the nonlinear buckles has been considered in an experimental approach for the DLC film under the equi-biaxial stressed thin film. At the condition for the straight-sided buckle, secondary bifurcation buckles, classified as varicose-type buckles and telephone cord buckles, have been observed along the side of the preexisting straight-sided buckle. For large widths, by contrast, the telephone cord buckle, as a nonlinear instability, has only been induced with a unique zigzag configuration, which reveals the bifurcation along the curved leading front as it grows (Figs. 7.1 and 7.4).

Fig. 7.4 Telephone cord buckling initiated from imperfections: interface defect (a) and free edge (b). Moon et al. [20], reprinted with permission



The two different formation sequences of telephone cord buckles have been compared with respect to buckle width. As well as the secondary bifurcation buckle from the straight side with a small perturbation on the preexisting simple straight-sided buckle with width b in the range of $2.0 < b/b_0 < 2.5$, where b_0 is the reference width for the onset of buckling, the nonsymmetric undulation has been observed with the bifurcation at the circular leading front in the natural growth range of $2.5 < b/b_0$ as the telephone cord expands. The characterization of telephone cord buckles has been provided by several equipment for measuring the exact morphologies, giving basic insight into further discussion about the energetic stability of telephone cord buckles. The axi-symmetric model for the nonlinear side of the telephone cord buckle has been compared with the straight side and circular front in terms of energy release rate and mode mixity.

The profiles of telephone cord buckles are characterized along different chords using the AFM. Images of the telephone cord buckles (Fig. 7.5) suggest that each repeated unit has a center of symmetry, denoted O in the figure, and that the circumference around that point, denoted by the arc XY, has constant curvature. The adjacent units have the inverse symmetry. Each repeated unit occupies roughly a 90° angular domain. AFM profiles measured along representative trajectories for

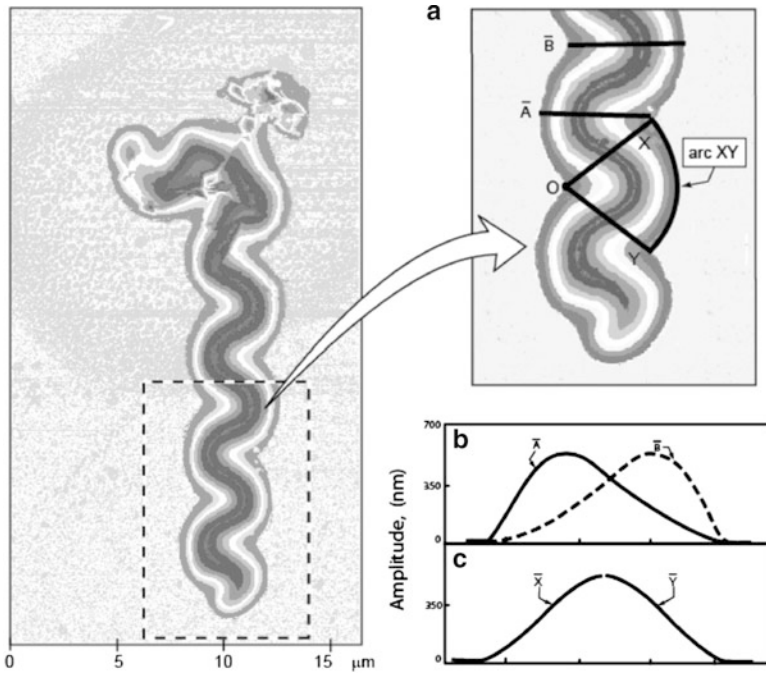


Fig. 7.5 Plan view of a telephone cord buckle, used to highlight a unit segment with the center of curvature at O and arc length XY (a). The profiles along the radial trajectories, A and B (b). The profile along the medians X and Y (c). Moon et al. [21], reprinted with permission

a DLC film (of thickness $h = 0.13 \mu\text{m}$) affirm the overall characteristics (Fig. 7.5a). *Radial trajectories* originating at O all have essentially the same asymmetric profile, exemplified by that shown in Fig. 7.5b. Note the mirror symmetry between A and B. Profiles along the medians between adjacent units (lines X and Y in Fig. 7.5a) are symmetric (Fig. 7.5c).

7.2.2.3 Energy Release Rate of Buckling

In order to estimate the energy relaxation during nonlinear buckle evolution, the full model of nonlinear buckle has been calculated for the nonlinear sides of telephone cord buckles, which reveals that telephone cord morphologies could release most of the strain energy as buckle widths or residual stress of the film increase. Besides telephone cord buckle as the nonlinear buckle morphology, the varicose type with symmetric instability along the side has also been predicted by the numerical calculation.

Given the symmetry of each unit of the telephone cord buckle, described above (see Figs. 7.1d and 7.5), it is assumed that the energy release rate and the profile can be modeled as a full circular buckle, of radius $r = R \equiv 2b$, with pinned center

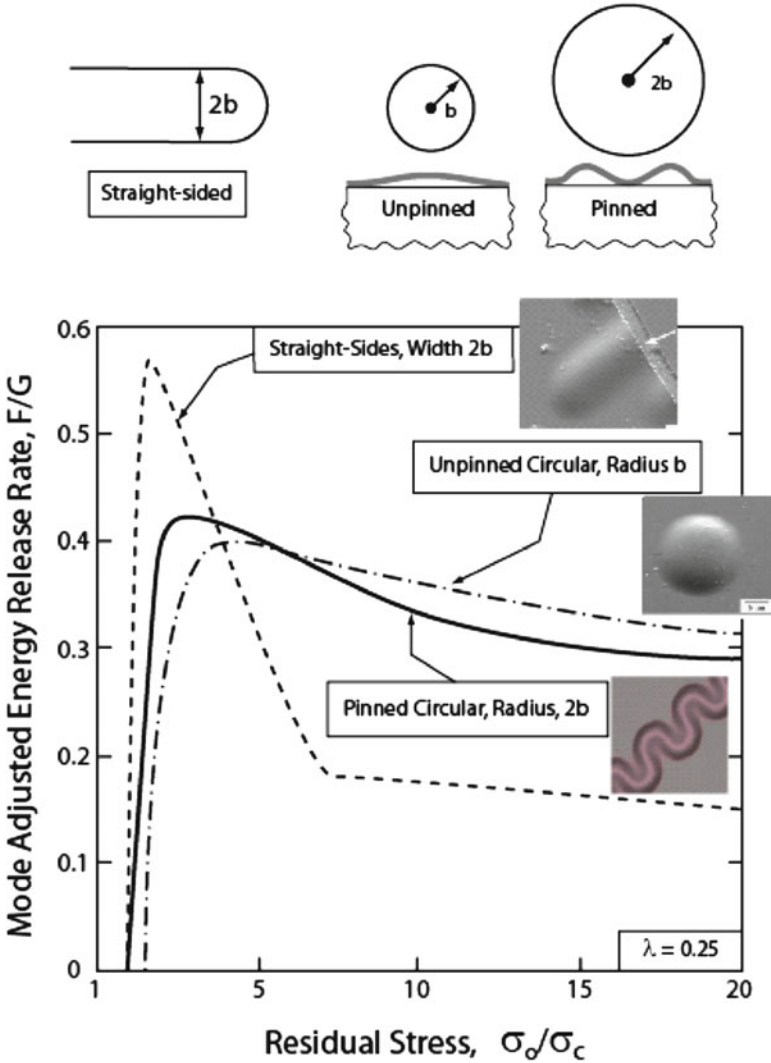


Fig. 7.6 The schematics for straight-sided (*top left and middle*) and telephone cord (*top right*) buckling used for analysis. Mode-adjusted energy release rate for three cases as a function of normalized film stress for three different morphologies. Moon et al. [21], reprinted with permission

(Fig. 7.6a). This assumption is validated below, using the measurements and analysis conducted for the straight-sided buckle created by the FIB. For a circular plate of radius $2b$ pinned to the substrate at the center, the corresponding critical stress is [5] $\sigma^* = 1.081\sigma_c$, and therefore only slightly greater than that of the straight-sided buckle of width $2b$.

Solutions for the circular, pinned buckle were obtained by numerical integration of the nonlinear, axi-symmetric von Karman equations [21]. The energy release rate and the phase angle are calculated using

$$G = \frac{1 - \nu^2}{2Eh^3} \left(12M^2 + h^2(N + \sigma_0 h)^2 \right) \quad (7.8)$$

and

$$\tan \psi = \frac{K_{II}}{K_I} = \frac{\sqrt{12M} \cos \omega + h(N + \sigma_0 h) \sin \omega}{-\sqrt{12M} \sin \omega + h(N + \sigma_0 h) \cos \omega}, \quad (7.9)$$

where the bending moment is $M = [Eh^3/(12(1 - \nu^2))]d^2w/dr^2$.

Computed results for G/G_0 and ψ for the pinned circular buckle used to model the sides of the telephone cord are presented in Fig. 7.6b as a function of σ_0/σ_c . The buckling stress, σ_c , for the straight-sided buckle of width $2b$, defined in (5.3), is used throughout to normalize the stresses. Included in Fig. 7.6b are the corresponding results for an unpinned circular buckle of radius b , obtained by numerical analysis [9, 12]. The buckling stress is $1.488\sigma_c$. To understand the trends at large σ_0/σ_c in Fig. 7.6, it is useful to identify the *total elastic energy per unit area* stored in the biaxially stressed film:

$$G_0^* = \frac{(1 - \nu)h\sigma_0^2}{E}. \quad (7.10)$$

Note that $G_0^*/G_0 = 1.54$ for a film with $\nu = 0.3$. As σ_0/σ_c becomes large, equivalent to a large-diameter buckle, the energy release rate slowly approaches G_0^* , asymptotically releasing all the stored energy in the film. The corresponding limit for the straight-sided buckle approaches G_0 , because the released film remains subject to the plane strain constraint parallel to the sides. For further assessment, it becomes convenient to express σ_0/σ_c in terms of the buckle size, b . For this purpose, a reference length is defined as the half-width of the straight-sided configuration at the onset of buckling,

$$b_0 \equiv \left(\frac{\pi}{\sqrt{12(1 - \nu^2)}} \right) h \sqrt{\frac{E}{\sigma_0}}, \quad (7.11)$$

whereupon

$$\frac{b}{b_0} = \sqrt{\frac{\sigma_0}{\sigma_c}}. \quad (7.12)$$

The energy release rates for the straight-sided, pinned, and circular buckles, summarized in Fig. 7.6, indicate that G and ψ for the circular buckle and at the sides of the telephone cord are similar. By comparison, G at the sides of the straight buckle is smaller, at least when the stress is large, $\sigma_0/\sigma_c \geq 9$ (as in the present case, addressed below). Moreover, when $\sigma_0/\sigma_c \geq 7.5$, the sides of the straight buckle experience pure mode II, while the circular buckles retain a substantial component of mode I.

The existence of the telephone cord morphology is intimately related to interfaces having toughness that increases with increasing proportion of mode II to mode I. Indeed, as revealed in earlier work [9, 12], the occurrence of stable propagation owes its existence to this mode dependence. The tendency to develop a curved delamination front is tied to the larger proportion of mode I relative to mode II as the buckle enlarges.

To simulate features of telephone cords with the solutions for circular and pinned circular buckles, it is useful to introduce a phenomenological representation of a family of interface toughness dependencies [9],

$$\begin{aligned}\Gamma_c(\psi) &= \Gamma_{Ic}f(\psi), \\ f(\psi) &= (1 + \tan^2((1 - \lambda)\psi)),\end{aligned}\tag{7.13}$$

where $\Gamma_c(\psi)$ is the mode-dependent interface toughness, Γ_{Ic} is the mode I toughness, and λ is a mode-sensitivity parameter that sets the strength of the mode dependence. The criterion for propagation of a crack in the interface is $G = \Gamma_c(\psi)$. The ratio of mode II to mode I interface toughness values is $\Gamma_{IIc}/\Gamma_{Ic} = 1 + \tan^2((1 - \lambda)\pi/2)$. Interfaces with moderately strong dependence typically have $\lambda < 0.3$ [6].

A mode-adjusted energy release rate, F , provides insight into the tendency of buckles to propagate on curved rather than straight edges [10]. With $\Gamma_c(\psi) = \Gamma_k f(\psi)$, let

$$F = \frac{G}{f(\psi)}\tag{7.14}$$

such that the criterion for propagation of the interface crack becomes $F = \Gamma_c$. Note that when σ_0/σ_c exceeds about 3 (or, equivalently, when $b/b_0 < \sqrt{3}$), the mode-adjusted energy release rate on the straight edge is lower than that on curved sides. This behavior underlies the tendency of highly stressed films to display curved buckle morphologies. It also explains why a straight-sided buckle propagates at its curved front, rather than spreading from its straight sides.

7.2.2.4 Strain Energy for Nonlinear Buckle

Confinement of a delamination buckle to a narrow strip of low adhesion (see next section) predetermines the width of the buckle and thereby eliminates the

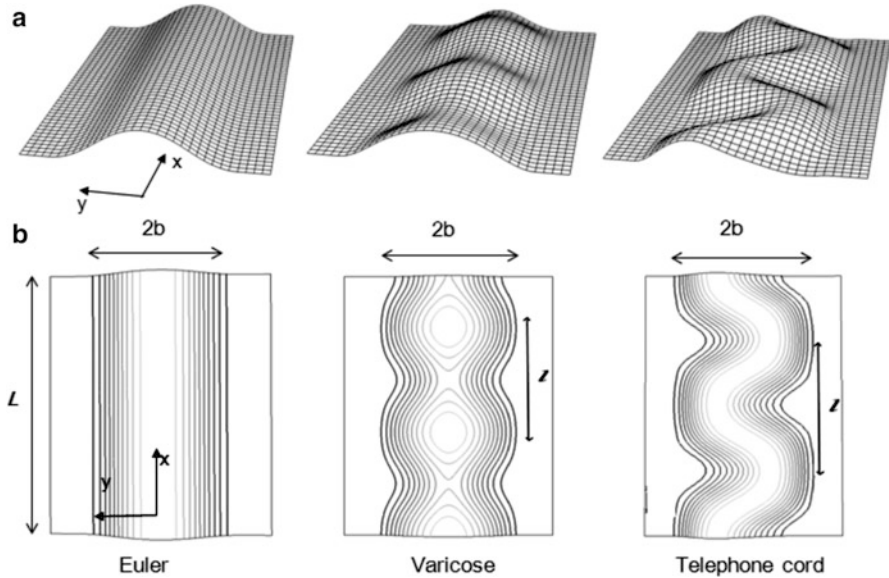


Fig. 7.7 Geometry and finite element mesh for buckling analysis of a constant width plate (film) clamped along its edges at $y = \pm b$ to a rigid substrate. The Euler mode, the varicose mode, and the telephone core mode are depicted in two views. Moon et al. [22], reprinted with permission

complicated role played by the mode dependence of the interface toughness in setting the buckle width for an unconfined delamination. The buckling and post-buckling behavior of a film under equi-biaxial compression that is detached from a substrate over a strip of width $2b$ is usually modeled as a plate of the same width that is fully clamped along its edges (Fig. 7.7). This is an excellent approximation for determining the critical stress, buckling amplitude, and relevant energy release rates as long as the Young's modulus of the substrate is not less than about one-fifth of that of the film [4, 30], as will be assumed here. When the substrate has a very low modulus compared to that of the film, deformation of the substrate along the edge of the detached region becomes important such that the assumption of a clamped edge overestimates the constraint.

The Euler mode has been used to compute the energy release rate along the sides of the buckle, but here the focus is on the energy release rate \bar{G} averaged over the curved end of the interface delamination crack propagating along the strip. For a strip of low adhesion of width $2b$, steady-state conditions at the propagating end prevail once the buckle delamination is several times longer than its width. The average energy release rate is simply the difference between the energy per area in the plate, U_0 , ahead of the propagating end (in the unbuckled state) and the average energy per unit area well behind the end in the buckled state, \bar{U} , i.e., $\bar{G} = U_0 - \bar{U}$. The energy per area in the unbuckled state of equi-biaxial compression is

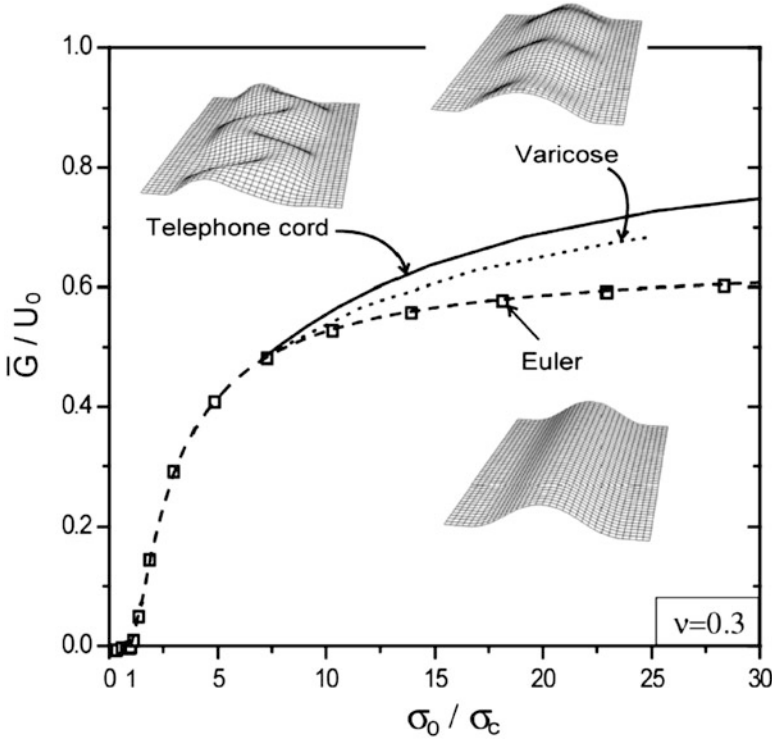


Fig. 7.8 Normalized average energy release rate for steady-state buckle delamination along a straight-sided strip, \bar{G}/U_0 , for each of the three buckle morphologies as a function of σ_0/σ_c and b/b_0 for $\nu = 0.3$. Moon et al. [22], reprinted with permission

$$U_0 = \frac{(1 - \nu)\sigma_0^2 h}{E} \tag{7.15}$$

while the average energy per area in the buckled state is found using (7.1)–(7.3) to be [9]

$$\bar{U} = U_0 \left(1 - \left(\frac{1 + \nu}{2} \right) \left(1 - \frac{\sigma_c}{\sigma_0} \right)^2 \right). \tag{7.16}$$

The energy release rate for the Euler mode is [9] $\bar{G} = G_0(1 - (\sigma_c/\sigma_0))^2$, where G_0 is from (7.6).

Plots of \bar{G}/U_0 for the Euler mode are included in Fig. 7.8, which will be introduced in the next subsection when the corresponding results for the two other morphologies are discussed. For each of the three modes, the normalized average energy release rate \bar{G}/U_0 is plotted in Fig. 7.8 based on the relation $\bar{G} = U_0 - \bar{U}$ or

$\bar{G}/U_0 = 1 - \bar{U}/U_0$ for $\nu = 0.3$. By considering $\bar{G} = G_{ss}$, the relation (7.7) for the Euler mode holds for $\sigma_0/\sigma_c < 6.5$ (or, equivalently, $b/b_0 < 2.5$) while the maximum energy release rate for $\sigma_0/\sigma_c > 6.5$ is associated with the telephone cord mode. For the telephone and varicose modes, \bar{G} is the energy release rate averaged over one complete wavelength of propagation. We speculate that \bar{G} will asymptotically approach the elastic energy per area stored in the unbuckled film, U_0 , as $\sigma_0/\sigma_c \rightarrow \infty$, but \bar{G}/U_0 has only attained 0.75 for $\sigma_0/\sigma_c = 30$. Note, however, that the telephone cord energy release rate \bar{G} exceeds the available energy per area subject to the plane strain constraint, $G_0 = (1 + \nu)U_0/2$, which is the asymptotic limit for the Euler mode. Results for \bar{G}/U_0 for the Euler mode and the telephone cord mode are presented in Fig. 7.8b for various Poisson's ratio values, showing that this normalization \bar{G}/U_0 for the telephone cord mode is relatively independent of Poisson's ratio at large values of σ_0/σ_c .

7.2.3 Buckle on the Patterned Substrate

Pre-patterned regions of low adhesion at the interface between the film and substrate constrain the delamination path and thereby give rise to more predictable behavior. When the regions of low adhesion are strips, as in Figs. 7.9 and 7.10, delaminations, once nucleated, propagate the full length of the strips if the strips are above a critical width. For reasons detailed below, the Euler mode emerges for the narrow strips while a morphology much like the telephone cord mode is preferred for the wider strips. In Fig. 7.9, buckle delaminations have been nucleated at the wide delaminated region at the top of the narrow strips of low adhesion and then have propagated from the top toward the bottom of the figure. As noted in Fig. 7.9, there are several strips that are too narrow for buckling delamination to occur, i.e., those having $2b \leq 6 \mu\text{m}$.

Both the Euler mode and a mode similar to telephone cord mode are in evidence in Fig. 7.9, where the patterned region of low adhesion is a tapered strip. The delamination has been nucleated at the wide end of the strip and has propagated toward the narrow end where it transitions to the Euler mode. While some features of the constrained mode depart from those of an unconstrained telephone cord, in most respects the two modes are remarkably similar and the term telephone cord mode will be used here to characterize the unsymmetric undulating mode [22]. Another notable feature seen in Fig. 7.9 is the arrest of the buckle delamination at a point where its width becomes too narrow to release sufficient energy to overcome the interface toughness.

In this part, the process for buckle patterning by lithography and adhesion controlling is discussed for DLC films deposited on patterned silicon wafer substrates. Selected experimental observations of buckle delamination of patterned regions of low adhesion are presented for several types of pattern. Analysis related

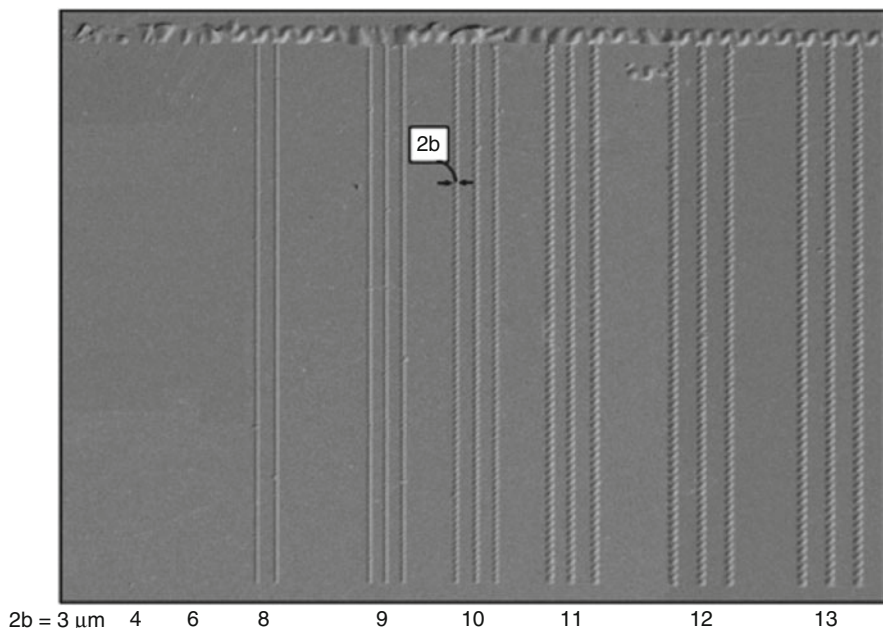


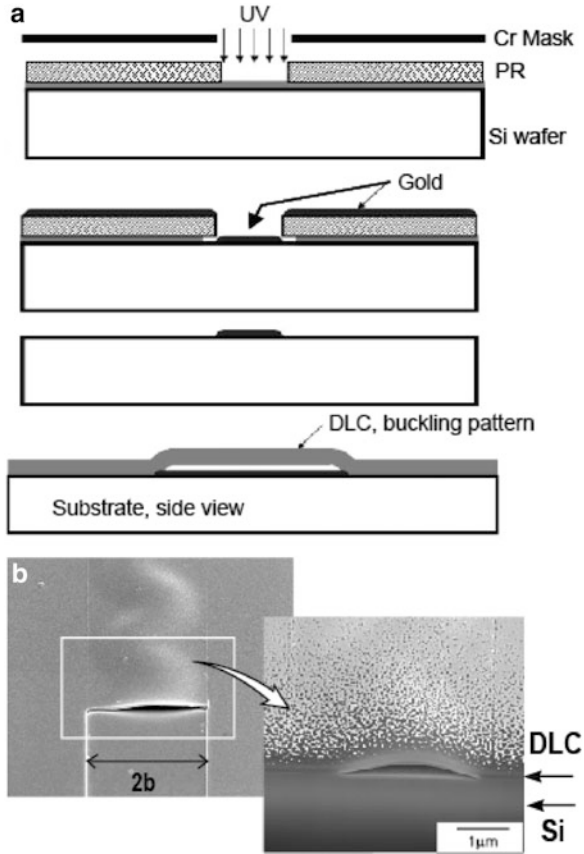
Fig. 7.9 Buckle delamination along patterned strips of low adhesion between a DLC film and a silicon substrate, showing the telephone cord morphology for wider strips and the Euler mode for narrower strips

to buckle patterning results was performed to assess strain energy and energy release rate for buckle morphologies elsewhere [24].

7.2.3.1 Patterning Experiments

The experimental procedure for patterning regions of low adhesion surrounded by regions of higher adhesion for DLC films on silicon substrates is briefly addressed with the aid of the schematic in Fig. 7.10. A 3 nm layer of Al_2O_3 between the Si and the DLC is used to create the regions of low adhesion. This layer is absent in regions of higher adhesion. The first step in creating the Al_2O_3 layer is to use E-beam lithography to expose the desired low adhesion pattern on the substrate (see Fig. 7.10). Standard lithography techniques in a clean room environment were employed. The positive E-beam resist (ER) layer was spin-coated on Si (100) followed by E-beam exposure of the regions selected for low adhesion. A very thin layer of Al is then sputter deposited which, upon oxidation, becomes an Al_2O_3 layer about 3 nm in thickness covering the low-adhesion regions. The ER layer covering the regions designated to have higher adhesion is removed with acetone and alcohol. The DLC layer is then deposited by the method of plasma-enhanced chemical vapor deposition (PECVD) using a *capacitively coupled r.f. glow*

Fig. 7.10 (a) Schematic for creating patterns of low adhesion and (b) a cross-sectional view of patterned buckling delamination. Moon et al. [24], reprinted with permission



discharge, choosing conditions that from prior experience will lead to buckle delamination. Here the DLC film thickness of 0.2–0.82 μm had residual compression between about 0.9 and 2 GPa in the equi-biaxial state [4, 21]. Although no direct observation of the location of the interface crack has been made, it can be believed that separation occurs either within the Al₂O₃ layer or at the interface between the Al₂O₃ and the DLC.

7.2.3.2 Buckle Delamination on Pattern with Constant Width

The basic pattern has been classified with respect to the various shapes of release layers: linear and tapered or network. When the buckle is confined by the linear shape of the release layer (the layer that has weak adhesion), the buckle morphologies are the same along the propagation direction due to the widths being identical in Fig. 7.11.

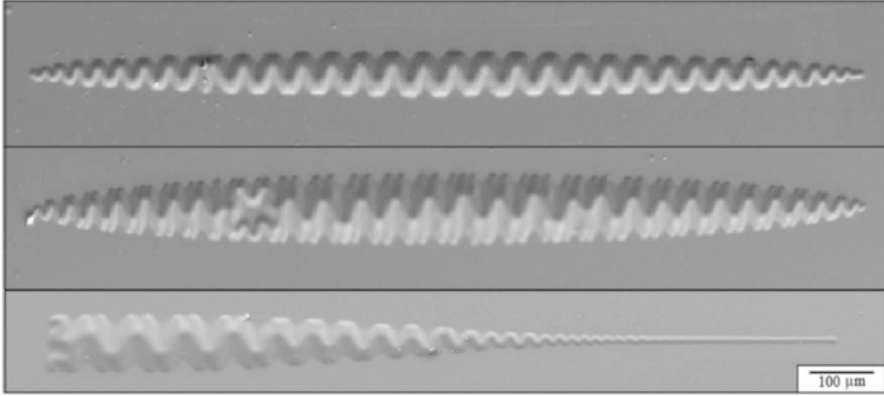


Fig. 7.11 Configuration of buckle delamination varying from straight-sided to telephone cord shape with respect to the pattern width on tapered low-adhesion layers. Moon et al. [22], reprinted with permission

Several design features of buckle patterns appear in Fig. 7.10, where the tapered release layer has been used for confinement of buckle width. As shown in the first feature in Fig. 7.10, the nonlinear side of the telephone cord buckle is unstable so that it shows the bifurcation phenomena along the nonlinear side at large width (mid of Fig. 7.10).

Regardless of buckle patterns, the configuration of buckle is shown to strongly depend on the buckle width. The array of buckle patterns shown in Fig. 7.11 could be applied for the micro (or nano) channels, which have a long tunnel inside the buckle [24]. By confinement of the buckle width to the 100 nm level, the channel with the nano-sized area could be developed, and some flows enable passing through the buckle tunnel.

7.2.3.3 Adhesion Measurement Using Buckling on Patterned Layer

Once nucleated, the condition for the buckle delamination to propagate along the strip is

$$\bar{G} \geq \Gamma_c. \quad (7.17)$$

The interface toughness, Γ_c , depends on the relative proportion of mode II-to-mode I stress intensity factors acting on the propagating interface crack front [1]. Methods to estimate the mode mix for buckle delaminations are presented in [21]. For an equi-biaxial compressive film stress σ_0 , very narrow strips with $\bar{G} < \Gamma_c$ will not delaminate. However, for wider strips with $\bar{G} > \Gamma_c$, buckle delaminations will propagate unimpeded (dynamically) along the strip once nucleated. Patterning strips of various widths provide a method to bracket the interface toughness

relevant to buckle delamination. *The toughness measured is that of the modified strip interface.* For the technique to be employed for measuring the toughness of a given film/substrate interface, the patterning procedure would have to be modified so as to enhance adhesion outside the strips without altering adhesion within the strip. This should be viable, at least for some interfaces, and will be pursued in subsequent work.

The DLC film on the silicon substrate in Fig. 7.10 nicely illustrates the method of bracketing Γ_c mentioned above for the strip interface. Based on the measurement techniques noted above, the DLC film in Figs. 7.9 and 7.11 is characterized with thickness, residual stress, and elastic modulus as $h = 0.26 \mu\text{m}$, $\sigma_0 = 1.4 \text{ GPa}$, $E = 100 \text{ GPa}$, $\nu \approx 0.3$. Then the onset width and the strain energies for undeformed and deformed films for (7.6) and (7.16) can be calculated to be $b_0 = 2.1 \mu\text{m}$, $U_0 = 3.57 \text{ Jm}^{-2}$, $G_0 = 2.32 \text{ Jm}^{-2}$, respectively. The width of the widest strip in Fig. 7.9 that did not delaminate is $2b = 6 \mu\text{m}$, which would correspond to $\bar{G} = 0.61 \text{ Jm}^{-2}$ had delamination occurred. Here the assumption is that the strip would have been wide enough to buckle had interface separation occurred, since $b > b_0$. The reason delamination does not occur is that insufficient energy is made available by interface separation, i.e., $\bar{G} < \Gamma_c$. The width of the narrowest strip that did delaminate (in the Euler mode) is $2b = 8 \mu\text{m}$, corresponding to $\bar{G} = 1.23 \text{ Jm}^{-2}$. Thus, the interface toughness governing the buckling delamination is bracketed by

$$0.61 \text{ Jm}^{-2} < \Gamma_c < 1.23 \text{ Jm}^{-2}. \quad (7.18)$$

A more refined determination is afforded by delamination along a tapered strip.

It should be noted that the propagation condition of (7.18) is necessary but not sufficient in the sense that the fracture condition is not enforced point-wise along the curved front of the delamination, but only as an average over the propagating front. If there is a significant variation of the mode mix from point to point on the propagating crack front, identification of Γ_c with \bar{G} produces the corresponding average of the interface toughness over the crack front. Point-wise estimation of the energy release rate and mode mix along the edge of a telephone cord delamination has been used to determine the interface toughness and associated mode mix of a Pt/SiO₂ interface [17]. The method was used to systematically explore the relation between one of the variables in the film deposition process and the interface toughness.

The theoretical prediction for the buckle amplitude from (7.2), i.e., $\xi = w_{\text{max}}/h = 1.52$ or $w_{\text{max}} = 394 \text{ nm}$, compares favorably with the experimental measurement, $w_{\text{max}} = 427 \text{ nm}$.

7.2.3.4 Buckle Delamination on Tapered Pattern Layer and Grid Networks

Adhesion release layers have been designed in network patterns as shown in Fig. 7.12. On the network channel of small width in each line (Fig. 7.12a), the

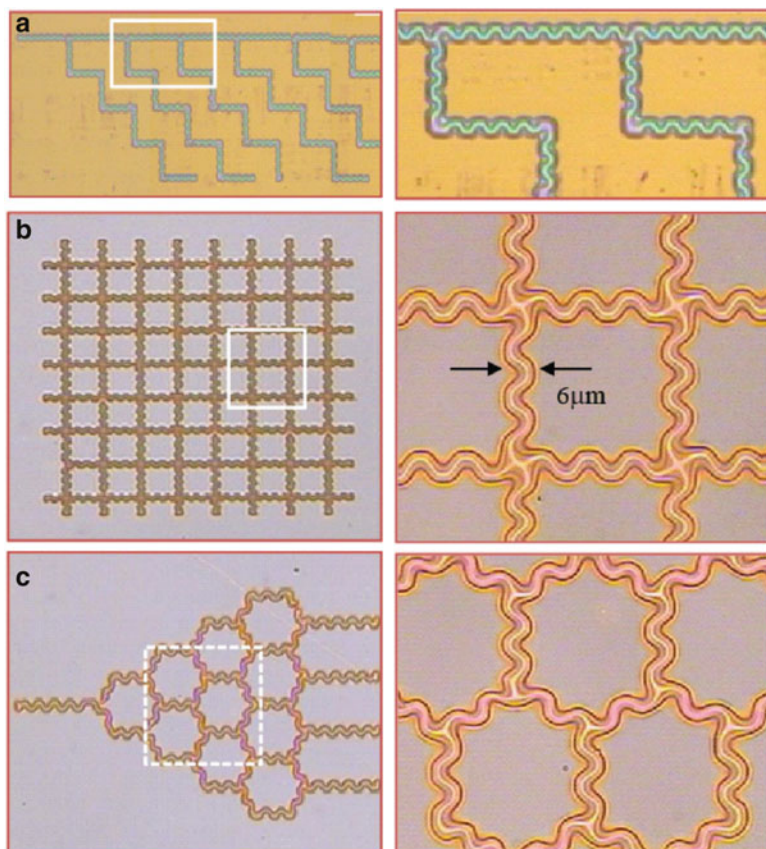


Fig. 7.12 Buckling patterns formed on various shapes of low-adhesion layer patterning. Moon et al. [24], copyright 2007 National Academy of Science, USA, reprinted with permission

straight-sided buckle grows and it passes across the next buckle branch at the junction, where the buckle is required to have fourfold symmetry, so straight-sided buckles at the junction are shown to be not stable due to there being no bifurcation mode in the Euler buckle during propagation. For the network with larger width (Fig. 7.12b), the telephone cord buckle also grows and passes across each junction. During propagation of the telephone cord buckle, it could introduce the bifurcation at the side or front so that the folding at the junction is relatively easy and it shows a stable buckle configuration at the junction as shown in Fig. 7.12b, c. In order to control and confine the buckle in a straight-sided shape at the network junctions, advanced design is required for junctions on the network.

New experiments into the control of buckle morphologies have been introduced by confinement of buckle width with interface adhesion differences. Films subject to equi-biaxial compression in the unbuckled state have been deposited on a patterned substrate. Highly controlled buckle delamination patterns and a wide

variety of buckle patterns can be achieved, such as straight channel-type buckles, tapered buckles, and buckle networks. The buckle configuration has been selected with respect to the confined buckle width. The straight-sided buckle, which is rarely observed in experimental conditions, has been stably shown on patterned layers with a small buckle width, but the buckle width for the existence of the straight-sided buckle is relatively narrow. As one can see it in usual buckle conditions, the telephone cord buckle appeared on relatively large widths. On the tapered pattern, two different buckle configurations of straight sided and telephone cord are formed. The propagation behavior on complex patterns of grids and corners has been also designed.

7.3 Summary

In this chapter, delamination buckle has been fully studied in experiments and the associated theory. The initiation of buckle delamination has been discussed in terms of interface defects or imperfections, where the criterion for the critical length that induces delamination or delamination buckle was presented. Once it initiates, the buckle grows in the form of a telephone cord buckle under usual experimental conditions. The characterization of buckle configurations has been dealt with by experiments and numerical modeling. Buckle patterns were introduced by confinement of the buckle width by means of controlling the interface adhesion on patterned substrates.

The buckle delamination has been characterized by experimental analysis and modeled to obtain a theoretical estimate of the energy state. The buckle could be developed by the confinement of buckle width, which is possible by interface adhesion control. In a later work, we demonstrated the possible applications of buckles on thin films in related fields such as nano-fluidics flowing through patterned buckles [24].

References

1. Audoly B (1999) Stability of straight delamination blisters. *Phys Rev Lett* 83(20):4124
2. Bowden N, Brittain S, Evans AG, Hutchinson JW, Whitesides GM (1998) Spontaneous formation of ordered structures in thin films of metals supported on an elastomeric polymer. *Nature* 393:146
3. Chen X, Hutchinson JW (2004) A family of herringbone patterns in thin films. *Script Mater* 50:797
4. Cho S-J, Lee K-R, Eun KY, J-h J, Kwon D (1999) A method of determining the elastic properties of diamond-like carbon films. *Diamond Relat Mater* 8:1067
5. Evans AG, Hutchinson JW (1984) On the mechanics of delamination and spalling in compressed films. *Int J Solid Struct* 20:455
6. Evans AG, Ruhle M, Dalgleish BJ, Charalambides PG (1990) The fracture energy of bimaterial interfaces. *Mater Sci Eng A*126:53

7. Faulhaber S, Mercer C, Moon M-W, Hutchinson JW, Evans AG (2006) Buckling delamination in compressed multilayers on curved substrates with accompanying ridge cracks. *J Mech Phys Solids* 54:1004
8. Gioia G, Ortiz M (1997) Delamination of compressed thin films. *Adv Appl Mech* 33:120
9. Hutchinson JW, Suo Z (1992) Mixed mode cracking in layered materials. *Adv Appl Mech* 29:63
10. Hutchinson JW (2001) Delamination of compressed films on curved substrates. *J Mech Phys Solids* 49(9):1847
11. Hutchinson JW, He MY, Evans AG (2000) The ratcheting of compressed thermally grown thin films on ductile substrates. *J Mech Phys Solids* 48:709
12. Hutchinson JW, Thouless MD, Liniger EG (1992) Growth and configurational stability of circular, buckling-driven film delaminations. *Acta Metal Mater* 40:295
13. Jensen HM, Sheinman I (2001) Straight-sided, buckling-driven delamination of thin films at high stress levels. *Int J Fract* 110:371
14. Kinbara A, Baba S, Matuda N, Takamisawa K (1981) Mechanical properties of and cracks and wrinkles in vacuum-deposited MgF_2 . *Thin Solid Films* 84:205
15. Kinbara A, Baba S (1991) Growth process of wrinkles generated in deposited films. *J Vac Sci Technol A* 9:2494–2496
16. Kim H-J, Moon M-W, Lee K-R, Seok H-K, Han S-H, Ryu J-W, Shin K-M, Oh KH (2008) Mechanical stability of the diamond-like carbon film on nitinol vascular stents under cyclic loading. *Thin Solid Films* 517:146–1150
17. Lee A, Clemens BM, Nix WD (2004) Stress induced delamination methods for the study of adhesion of Pt thin films to Si. *Acta Mater* 52(7):2081
18. Lee K-R, Baik Y-J, Eun K-Y (1993) Stress relief behaviour of diamond-like carbon films on glasses. *Diamond Relat Mater* 2:218
19. Matuda N, Baba S, Kinbara A (1981) Internal stress, Young's modulus and adhesion energy of carbon films on glass substrates. *Thin Solid Films* 81:301
20. Moon M-W, Chung J-W, Lee K-R, Oh KH, Wang R, Evans AG (2002) An experimental study of the influence of imperfections on the buckling of compressed thin films. *Acta Mater* 50:1219
21. Moon M-W, Jensen HM, Oh KH, Hutchinson JW, Evans AG (2002) The characterization of telephone cord buckling of compressed thin films on substrates. *J Mech Phys Solids* 50 (11):2355
22. Moon M-W, Lee K-R, Oh KH, Hutchinson JW (2004) Buckle delamination on patterned substrates. *Acta Mater* 52(10):3151
23. Moon M-W, Lee SH, Sun JY, Oh KH, Vaziri A, Hutchinson JW (2007) Wrinkled hard skins on polymers created by focused ion beam. *Proc Natl Acad Sci U S A* 104:1133
24. Moon M-W, Chung S, Lee K-R, Oh KH, Stone HA, Hutchinson JW (2007) Directed assembly of fluidic networks by buckle delamination of films on patterned substrates. *Int J Mater Res* 12:1203–1208
25. Ogawa K, Ohkoshi T, Tekeuchi T, Mizoguchi T, Masumoto T (1986) Nucleation and growth of stress relief patterns in sputtered molybdenum films. *J Appl Phys* 25:695
26. Pundt A, Nikitin E, Pekarski P, Kirchheim R (2004) Adhesion energy between metal films and polymers obtained by studying buckling induced by hydrogen. *Acta Mater* 52:1579
27. Thouless MD (1993) Combined buckling and cracking of films. *J Am Ceram Soc* 76(11):2936
28. Tolpygo VK, Clarke DR (2000) Spalling failure of α -alumina films grown by oxidation: I. Dependence on cooling rate and metal thickness. *Mater Sci Eng A* 278:151
29. Weissmantel GHR, Schurer C, Frohlich F, Grau P, Lehmann H (1979) Mechanical properties of hard carbon films. *Thin Solid Films* 61(2):L5
30. Yu HH, Hutchinson JW (2002) Influence of substrate compliance on buckling delamination of thin films. *Int J Fract* 113:39